



## Research article

# Didactic model of a simple driven microwave resonant T-L circuit for chaos, multistability and antimonotonicity



F.C. Talla<sup>a,b,c</sup>, R. Tchitnga<sup>a,b,d,\*</sup>, R. Kengne<sup>a,b</sup>, B. Nana<sup>c</sup>, A. Fomethé<sup>e</sup>

<sup>a</sup> Research Group on Experimental and Applied Physics for Sustainable Development, Faculty of Science, Department of Physics, University of Dschang, P.O.Box 412, Dschang, Cameroon

<sup>b</sup> Unit of Condensed Matter Research, Electronics and Signal Processing, LAMACET, Faculty of Science, Department of Physics, University of Dschang, P.O. Box 67, Dschang, Cameroon

<sup>c</sup> Department of Physics, Higher Teacher Training College, University of Bamenda, P.O. Box 39, Bamenda, Cameroon

<sup>d</sup> Institute of Surface Chemistry and Catalysis, University of Ulm, Albert-Einstein-Allee 47, Ulm, 89069, Germany

<sup>e</sup> Laboratoire de Mécanique et de Modélisation des Systèmes, L2MS, Department of Physics, Faculty of Science, University of Dschang, P.O.Box 67, Dschang, Cameroon

## ARTICLE INFO

## Keywords:

Education  
Electrical engineering  
Nonlinear physics  
Antimonotonicity  
Bipolar junction transistor  
Chaos  
Didactic model  
High frequency  
Multistability  
Parasitic capacitance

## ABSTRACT

A simple driven bipolar junction transistor (BJT) based two-component circuit is presented, to be used as didactic tool by Lecturers, seeking to introduce some elements of complex dynamics to undergraduate and graduate students, using familiar electronic components to avoid the traditional black-box consideration of active elements. Although the effect of the base-emitter (BE) junction is practically suppressed in the model, chaotic phenomena are detected in the circuit at high frequencies (HF), due to both the reactant behavior of the second component, a coil, and to the birth of parasitic capacitances as well as to the effect of the weak nonlinearity from the base-collector (BC) junction of the BJT, which is otherwise always neglected to the favor of the predominant but now suppressed base-emitter one. The behavior of the circuit is analyzed in terms of stability, phase space, time series and bifurcation diagrams, Lyapunov exponents, as well as frequency spectra and Poincaré map section. We find that a limit cycle attractor widens to chaotic attractors through the splitting and the inverse splitting of periods known as antimonotonicity. Coexisting bifurcations confirm the existence of multi-stability behaviors, marked by the simultaneous apparition of different attractors (periodic and chaotic ones) for the same values of system parameters and different initial conditions. This contribution provides an enriching complement in the dynamics of simple chaotic circuits functioning at high frequencies. Experimental lab results are completed with PSpice simulations and theoretical ones.

## 1. Introduction

Introducing complex dynamics in electronics at undergraduate level can be demanding, when complex electronic devices and complex mathematical formulas are in use. To overcome the didactic barrier that can result from too complex components, black-box models are often used, so that only the mathematical output functions of various blocs are considered. This hinders sometimes students to go deep in the understanding of the physics beyond the black-boxes. In the present paper, we use two components that are very familiar to students, to give a tool that can help to uncover the origin of complex phenomena often found in very complex circuits. This is like “opening” the black-box for undergraduates, hoping to inspire engineering skills in them.

In 2002, Aissi proposed an autonomous Colpitts oscillator and a

driven RL-Diode circuit as examples of chaotic circuits for undergraduates [1]. His paper was limited on the basics. The schema was not analyzed in term of equivalent circuit. A few years later, Perc used nonlinear time series analysis in a more consistent paper for a similar purpose [2]. Those two contributions confirmed that the subject can be introduced at that educational level.

The present paper goes more in details. It is understood as *helping tools* for didactic purpose. Dynamic systems to be characterized as chaotic must be third or higher-order nonlinear differential equations, or driven second or higher-order ones, with at least one positive Lyapunov exponent [3]. Since Lorenz [4] found the first chaotic attractor in 1963 while describing the simplified Rayleigh–Benard problem, the theory of chaos has obtained recognition in many fields of science and engineering. It can be encountered in medicine [5], in chemistry [6] in electromechanical

\* Corresponding author.

E-mail address: [robert.tchitnga@eaphysud.org](mailto:robert.tchitnga@eaphysud.org) (R. Tchitnga).

<https://doi.org/10.1016/j.heliyon.2019.e02715>

Received 20 June 2019; Received in revised form 30 July 2019; Accepted 21 October 2019

2405-8440/© 2019 Hydrogen Energy Publications LLC. Published by Elsevier Ltd. All rights reserved.

[7, 8, 9] and in optical systems [10], in control, secure communications and crypto systems [11, 12, 13], or in neurosystems [14, 15], just to name some. One of the most active fields for chaos and applications remains that of electronic circuits. Apart from the groundbreaking Chua's circuit [3], many other chaotic circuits have been found, or existing oscillators used to introduce sinusoidal oscillations in curricula have been modified for chaos [16, 17, 18, 19, 20, 21], so that proposing new circuits can now make sense according to Sprott [22], only if they fulfill at least one of the following requirements:

- (i) Credibly modeling some important unsolved problem in nature and shed insight on that problem;
- (ii) Exhibiting some behavior previously unobserved or
- (iii) Being simpler than all other known examples exhibiting the observed behavior.

Recently, Ref. [16] presented a Hartley's chaotic oscillator based on one JFET and one tapped coil, qualified as the simplest chaotic circuit, with experimental realization. The authors demonstrated that their circuit generates chaotic oscillations through periods doubling scenarios. However, the phenomena of antimonotonicity and multistability were not revealed in that simple circuit. Two other research groups proposed other simple chaotic circuits based on a nonlinear active memristor [23, 24]. They too showed attractors from their respective circuits along with an illustration of period doubling route to chaos. But for experimental realization, commercial memristors are not yet very accessible, obliging the used of analog calculators in most of the cases and therefore, many components to realize it [23, 24, 25, 26]. The present circuit combines simplicity both in the topology and in the realization.

Authors of some pioneering diodes or transistors based driven simple circuits [1, 27, 28, 29] have ignored the high frequency (HF) behavior of these nonlinear elements. In our case, this aspect is rather essential to justify and explain how an effective two-component circuit with only one physically observable degree of freedom can turn into multistable dynamics. Complementary virtual degrees of freedom needed for chaos finds their origin in the Giacoletto description of the "strange" behavior of semiconductors' junctions at high frequencies [30], known as parasitic capacitances. On the other hand, HF chaotic sources are imperative in many telecommunication applications, including broadband communications, broad-spectrum techniques, high-entropy source cryptography, etc... that require carriers at high frequency. The design of such systems requires a more detailed description of its elements and a precise characterization of the spectral band of the sources. The literature gives examples of experimental chaotic circuits operating in the microwaves domain [31] and [32], but with reduced details in modeling and analysis. The use of a bipolar junction transistor as active and nonlinear element of our circuit is justified by its characteristics and availability for any scholar: small size, low cost, low power dissipation, possible operation at HF, high current drive and high reliability in severe environmental conditions for engineering applications. It is therefore advisable to avoid as far as possible the reduced equivalent circuits of BJTs when the frequency of the circuit is in the range of MHz and higher, which are rather suitable at low frequencies. In the following, we are going to consider the global equivalent defined in Ref. [31].

The BJT-coil circuit of the present paper has a zero BE voltage and only the effect of BC junction gives rise to rich chaotic oscillations. The model, although simple, works at resonant frequencies in the range of microwaves. From the equations that describe the dynamics of this system, a study of the stability and the performances of the system in HF are done. Chaotic motions are justified using the Lyapunov exponent, bifurcations diagrams and Poincaré map section. This extremely simple circuit has a particular and significant imprint of multi-stability marked by the coexistence of different (periodic and chaotic) attractors obtained with the same values of system parameters on the different initial

conditions. The experimental and analogical analyses on the proposed simple driven circuit are also carried out to confirm our theoretical results.

The structure of the paper foresees in Section 2 the model description followed by the stability analysis in Section 3. In the next section, the experimental setup and PSpice simulation are depicted whereas numerical investigations are proposed in Section 5, just before the conclusion in the last section.

## 2. Design

### 2.1. Description of the circuit

Fig. 1 depicts the resonant circuit consisting of a BJT with short-circuited BE electrodes, and a coil. This circuit, in the absence of the driving force cannot generate oscillations, even in the presence of a biasing direct voltage source connected at the collector of the BJT, since the circuit has no feedback loop. The possible control parameters accessible to any experimenter can be the sinusoidal voltage source driving the circuit, and the inductance  $L$  of the coil that can be chosen as variable component.

### 2.2. Model and theoretical analysis

Many equivalent models of BJTs do exist in the literature [31, 32, 33, 34, 35, 36, 37]. One of the most appropriate for our study is the hybrid- $\pi$  model for frequencies up to 500 MHz. Fig. 2 shows the complete equivalent circuit of the proposed circuit (Fig. 1) using the modified equivalent hybrid- $\pi$  transistor model presented in [35], which takes into account:

- the BE capacity  $C_{BE}$ . (this capacity is the sum of a depletion capacity, that of diffusion proportional to the emitter current and of the transition capacity);
- the BC capacity  $C_{BC}$ , which essentially depends on the BC voltage;
- the base distributed resistance  $R_B$  (linear and measurable resistance, independent of the oscillation frequency), and
- the active internal resistance  $R_C$  of the collector's region.

The dynamic operation of the BJT is modeled by diffusion and depletion layer components. Consider  $v_{BE}$  the voltage across the capacitor  $C_{BE}$ ,  $v_{BC}$  the voltage across the capacitor  $C_{BC}$  and  $i_L$  the current through the coil with inductance  $L$ .

Kirchhoff's laws applied to the small-signal equivalent circuit in Fig. 2 lead to the system of ordinary differential equations (ODEs) below describing the complete dynamics of our circuit:

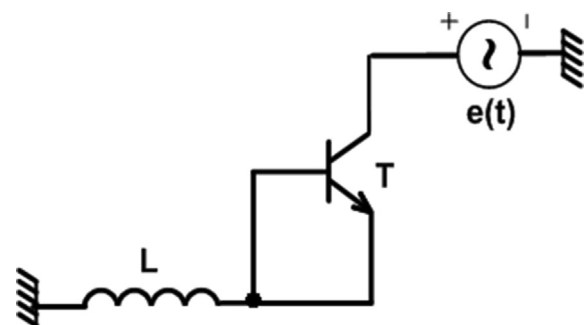


Fig. 1. Circuit diagram of the proposed driven two components oscillator;  $e(t) = E \sin(2\pi ft)$  is a sinusoidal source with amplitude  $E$  and frequency  $f$ ,  $T$  is the bipolar junction transistor and  $L$  is the inductance of the coil.

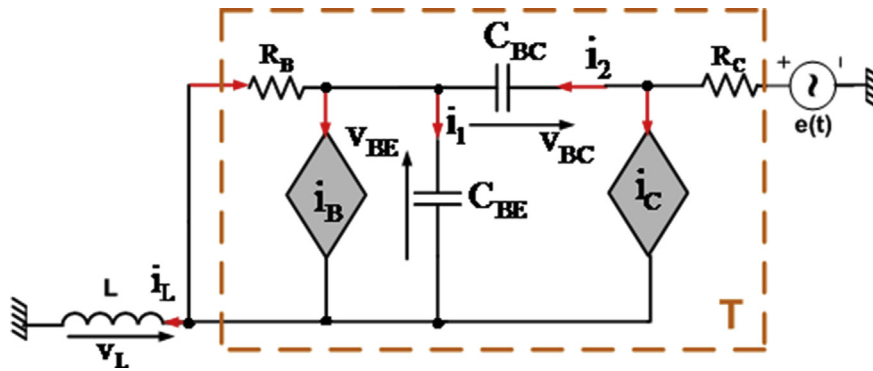


Fig. 2. Complete Small-signal equivalent circuit of the proposed two components driven oscillator.  $i_B$  and  $i_C$  are the voltage controlled current sources (VCCS).

$$\begin{cases} C_{BE} \frac{dv_{BE}}{dt} = -\left(\frac{1}{R_B}\right)v_{BE} + i_L - (i_B + i_C) \\ C_{BC} \frac{dv_{BC}}{dt} = i_L - i_C \\ L \frac{di_L}{dt} = -(v_{BE} + v_{BC}) - R_C i_L + E \sin(2\pi ft) \end{cases} \quad (1)$$

In several works the expression of current in the transistor is a function of the voltage between the base and the emitter [13, 16, 17, 18, 21, 31, 32, 36]. But this is actually a simplified form and can hide some phenomena. The general shape of currents in transistors take into account both the BE junction effects and the BC one as considered in Eqs. (2) and (3). Here the current sources  $i_B$  and  $i_C$  are controlled by the BE and the BC voltages ( $v_{BE}$ ,  $v_{BC}$ ):

$$i_B = f(v_{BE}, v_{BC}) = \frac{I_s}{\beta_F} \left[ \exp\left(\frac{v_{BE}}{V_T}\right) - 1 \right] + \frac{I_s}{\beta_R} \left[ \exp\left(\frac{v_{BC}}{V_T}\right) - 1 \right], \quad (2)$$

$$i_C = g(v_{BE}, v_{BC}) = I_s \left[ \exp\left(\frac{v_{BE}}{V_T}\right) - 1 \right] + I_s \left[ \exp\left(\frac{v_{BC}}{V_T}\right) - 1 \right] - \frac{I_s}{\beta_R} \left[ \exp\left(\frac{v_{BC}}{V_T}\right) - 1 \right] \quad (3)$$

where  $V_T = K_b T/q$ ,  $I_s$  is the reverse saturation current,  $T$  the junction absolute temperature,  $q$  the electrical charge,  $K_b$  the Boltzmann constant,  $v_{BE}$  and  $v_{BC}$  denoting the BE and the BC voltages respectively. Note that  $V_T \approx 26$  mV at the ambient temperature (300 K).

In order to highlight the vectors of nonlinear behavior of the functions  $f(v_{BE}, v_{BC})$  and  $g(v_{BE}, v_{BC})$ , let us note here the dependence of the saturation current  $I_s$  with respect to certain quantities such as the density of the charge carriers (efficiency injection), the substrate dimensions and the diffusion constant. Thus, the reverse saturation current takes the form

$$I_s = \frac{q^2 n_i A_0 D_{nb}}{Q_B} \quad (4)$$

Here  $A_0$  represents the emitter area,  $n_i$  is the concentration of the intrinsic carriers in the base and  $D_{nb}$  denotes the average diffusion constant of the minority carriers in the Base.  $Q_B$  is the charge per unit area of doped atoms in the neutral base. This charge density can be defined as

$$Q_B = q \int_{x_E}^{x_C} N_{ab}(x) dx. \quad (5)$$

$N_{ab}$  is the doping concentration in the base,  $x_C$  and  $x_E$  are spatial coordinates that delimit the neutral base with zero bias. It should be emphasized that these limits vary according to the junction voltages, giving rise to a so-called basic width modulation phenomenon.

Assuming some changes of variables and parameters as in Eq. (6), the dimensionless system of ODEs (7), suitable for numerical simulations, is obtained:

$$\begin{aligned} v_{BE} &= x \quad V_0; \quad v_{BC} = y \quad V_0; \quad i_L = z \frac{V_0}{\rho}; \quad \rho = \sqrt{\frac{L}{C_1}}; \quad \gamma = \frac{\rho I_0}{V_0}; \quad \alpha_B \\ &= \frac{\rho}{R_B}; \quad \alpha_C = \frac{\rho}{R_C}; \quad e = \frac{E}{V_0}; \quad \mu = \frac{\omega}{\omega_0}; \quad \in \\ &= \frac{C_{BE}}{C_{BC}}; \quad t = \tau \sqrt{LC_{BE}} \end{aligned} \quad (6)$$

and

$$\begin{cases} \dot{x} = -\alpha_B x + y - \gamma(f(x, y) + g(x, y)) \\ \dot{y} = \in(z - \gamma g(x, y)) \\ \dot{z} = e \sin(\mu \tau) - (x + y + z/\alpha_C). \end{cases} \quad (7)$$

Here the nonlinear functions are given by Eq. (8):

$$\begin{aligned} f(x, y) &= \alpha_1(e^x - 1) + \alpha_2(e^{-y} - 1), \quad \text{and} \quad g(x, y) \\ &= (e^x - 1) - (1 - \alpha_2)(e^{-y} - 1). \end{aligned} \quad (8)$$

The complete dynamic of the system can be investigated through the system of first order nonlinear differential Eq. (7) with (8).

### 3. Theory

The equations of the system can be written as the smooth nonlinear third order differential equation:

$$\frac{dX}{dt} = h(X, t, P); \quad t \in \mathbb{R}; \quad X \in \mathbb{R}^n \quad \text{and} \quad p \in \mathbb{R}^r. \quad (9)$$

$X = [x, y, z]^T$  is the vector field of states' variables.

$h(X, t, P) = [f_1(X, t, p), f_2(X, t, p), f_3(X, t, p)]^T$  is a smooth function and  $P = h(\alpha_B, \alpha_C, \gamma, \in, \mu, e)$  are the elements of the parameter space.

The fixed points of system (7) or (9) can be found by solving the nonlinear system (10), after cancelling the effect of the external driven source,

$$h(X, t, P) = 0. \quad (10)$$

This leads to the origin as unique equilibrium point of the present system:  $E_0(0, 0, 0)$ .

The perturbation analysis described in [38] is used to investigate the stability of solutions around the fix point  $E_0$ . Thus, Eq. (7) can be perturbed by adding a small perturbation  $\delta X = (\delta x, \delta y, \delta z)$  to the steady state  $X_0 = (x_0, y_0, z_0)$ . The dynamic differential Eq. (11) at the equilibrium point  $E_0(0, 0, 0)$  is obtained:

$$\frac{d\delta X}{dt} = M_J \delta X \tag{11}$$

Where  $M_J$  is a  $3 \times 3$  Jacobian matrix giving in Eq. (12) that describes the vector field along the solution  $\delta X(t)$ :

$$M_J = \begin{pmatrix} -\alpha_B - \gamma(1 + \alpha_1)e^x & \gamma(2\alpha_2 - 1)e^{-y} & 1 \\ -\epsilon \gamma e^x & -\epsilon \gamma(1 - \alpha_2)e^{-y} & \epsilon \\ -1 & -1 & -1/\alpha_C \end{pmatrix}. \tag{12}$$

At the equilibrium point  $E_0(0, 0, 0)$ ,  $M_J$  becomes:

$$M_{J(E_0)} = \begin{pmatrix} -\alpha_B - \gamma(1 + \alpha_1) & \gamma(2\alpha_2 - 1) & 1 \\ -\epsilon \gamma & -\epsilon \gamma(1 - \alpha_2) & \epsilon \\ -1 & -1 & -1/\alpha_C \end{pmatrix}. \tag{13}$$

The corresponding characteristic equation is

$$A_0 \lambda^3 + A_1 \lambda^2 + A_2 \lambda + A_3 = 0, \tag{14}$$

where the coefficients  $A_0, A_1, A_2$  and  $A_3$  are defined as:

$$\begin{aligned} A_1 &= \epsilon \gamma(1 - \alpha_2) + \gamma(1 + \alpha_1) + \alpha_B + \frac{1}{\alpha_C}, \\ A_3 &= (-\alpha_B - \gamma - \gamma \alpha_1) \left( \frac{\epsilon \gamma}{\alpha_C} - \frac{\epsilon \gamma \alpha_2}{\alpha_C} + \epsilon \right) - \epsilon \gamma \alpha_2, \\ A_0 &= 1, \quad A_2 = (1 - \alpha_2) \left( \epsilon \gamma \alpha_B + \epsilon \gamma^2 \alpha_1 + \frac{\epsilon \gamma}{\alpha_C} \right) \\ &+ \frac{\gamma}{\alpha_C} (1 + \alpha_1) + \frac{\alpha_B}{\alpha_C} + \epsilon - 1. \end{aligned} \tag{15}$$

The analysis shows that the coefficients  $A_0, A_1$  and  $A_2$  are positive while the coefficient  $A_3$  is negative; thus the system is unstable around the fixed point  $E_0(0, 0, 0)$  according to the Routh-Hurwitz criterion. It should be noted that the system may change the behavior under the effect of the external driven voltage source.

The analysis of the steady states and the local bifurcations susceptible to occur in our system when varying the parameters is done by solving Eq. (14) using the Newton-Raphson method, for the parameters' values  $\alpha_B = 0.0988, \alpha_C = 0.3953, \gamma = 4.9411, \alpha_1 = 0.3, \alpha_2 = 2.95$  and  $\epsilon$  in the range  $0 \leq \epsilon \leq 5$ . The graphical results are depicted in Fig. 3. From this figure it is observed that the roots of characteristic Eq. (14) include complex conjugate with negative and positive real parts, pure positive and negative real numbers, and pure imaginary numbers. It

then gives an idea on both the stability of periodic solutions as well as different types of bifurcation likely to appear in the system [38, 39]. Thus for the eigenvalues  $\lambda$  with all negative real parts, the rate is of contraction type, else of expansion's. For the pure real eigenvalues, contraction or expansion is observed near the steady state while contraction or expansion of spirals is observed for complex eigenvalues of the Jacobian matrix. For the eigenvalues having real parts with different sign, the equilibrium state is called saddle; an equilibrium point whose eigenvalues have nonzero real parts is called hyperbolic while we have a center if the eigenvalues are complex conjugate with zero real part (this is one of the conditions for Hopf type bifurcation to occur). By setting  $\lambda = -1$  in Eq. (14), we can find the value of the control parameter for which period doubling bifurcation type is obtained.

### 4. Experimental

Fig. 4 depicts the real experimental implementation of the circuit in Fig. 1 using a transistor of type BC107 and a self-inductance  $L = 75\mu H$ . The circuit is not biased and therefore, it is not an oscillator. Furthermore, it possesses no effective feedback loop and cannot oscillate, even if it were biased with a DC voltage source. Instead, it is a nonlinear resonant circuit driven by a Voltcraft TNG 235 sinusoidal voltage generator which provides the necessary energy to the system. The experimental chaotic  $(+e(t), v_B)$ -phase portrait is displayed at the frequency  $f \approx 4.87$  MHz and amplitude  $E \approx 5V$ . The graphical result on the figure was visualized on a dual channel 20 MHz HM 205-3 Hameg oscilloscope. Similar experiment via PSpice simulations gave the  $(i_L, v_B)$ -phase diagrams in Fig. 5 for the same Transistor and inductance value, the driven source having a frequency of 5MHz and amplitude of 4.5V. It is worth mentioning that other transistor types (e.g. BC108, Q2N222A etc...) have given almost similar results. This generator plays at the same time the role of control parameter through the variation of its frequency or its amplitude.

### 5. Results & discussion

#### 5.1. Method and detection of chaos

The numerical simulations for the investigations of the system's behavior were done in MatLab environment, using the four-order Runge-Kutta (RK4) algorithm. For the fixed set of parameters' values,  $\alpha_B =$

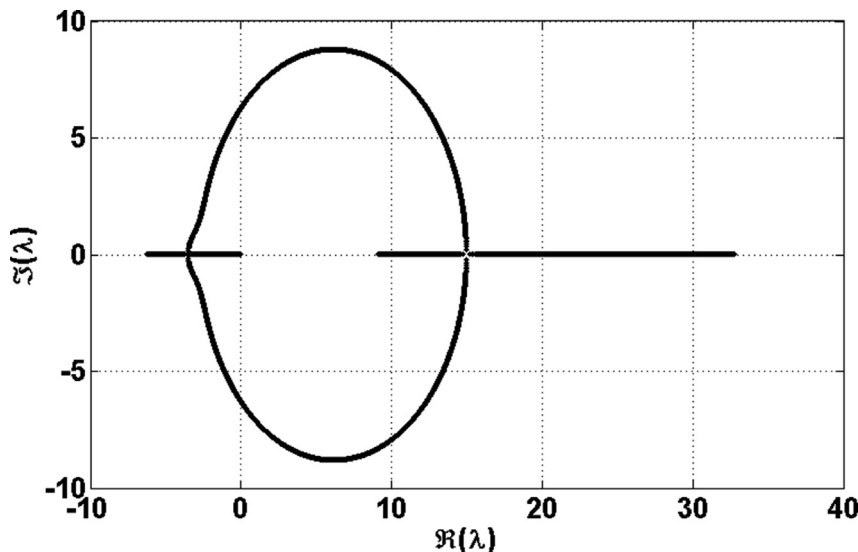


Fig. 3. Representation of the eigenvalues solutions of (14) in the complex plane ( $Re(\lambda), Im(\lambda)$ ). The parameters' values are  $\alpha_B = 0.0988, \alpha_C = 0.3953, \gamma = 4.9411, \alpha_1 = 0.3, \alpha_2 = 2.95$  and  $0 \leq \epsilon \leq 5$ .

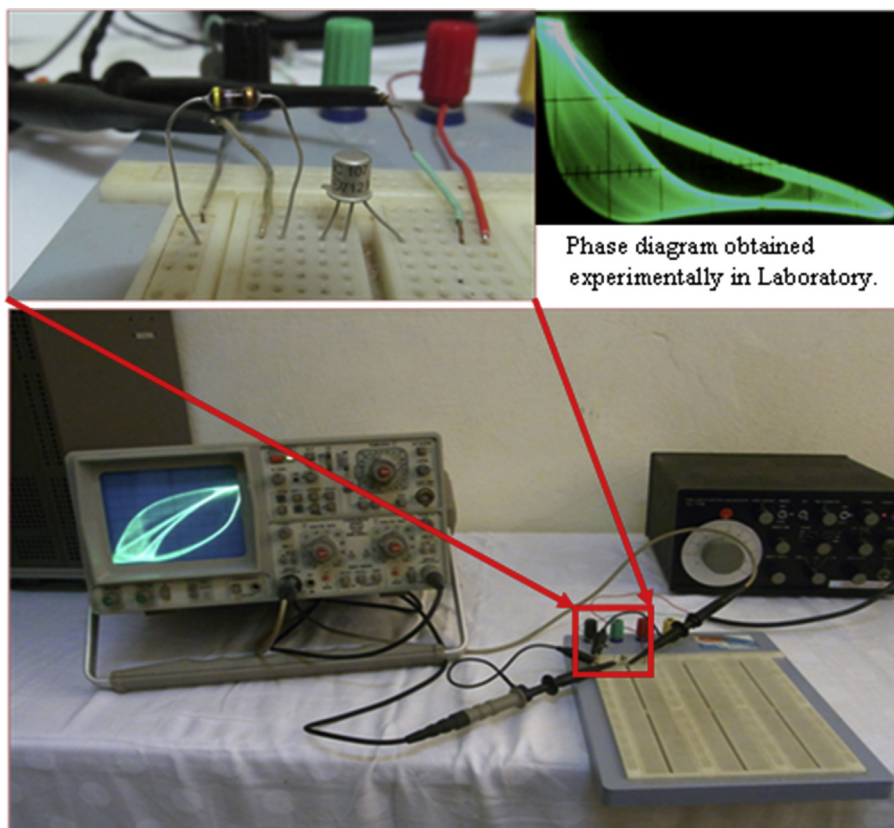


Fig. 4. Experimental setup of the BC107-type BJT based two components circuit in operation. The oscilloscope displays the double-band chaotic attractor captured from the experimental circuit mounted on a breadboard as indicated in the same figure.

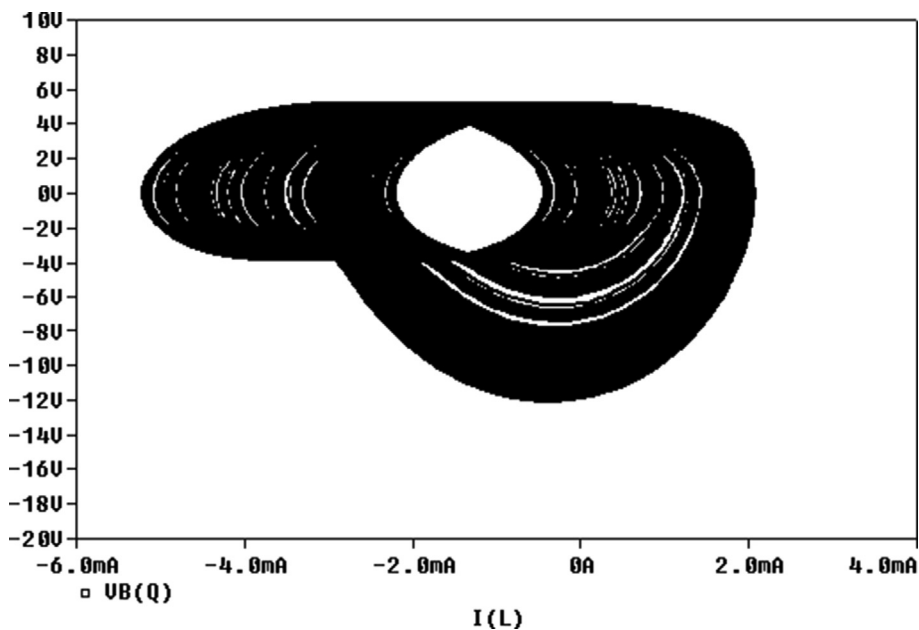
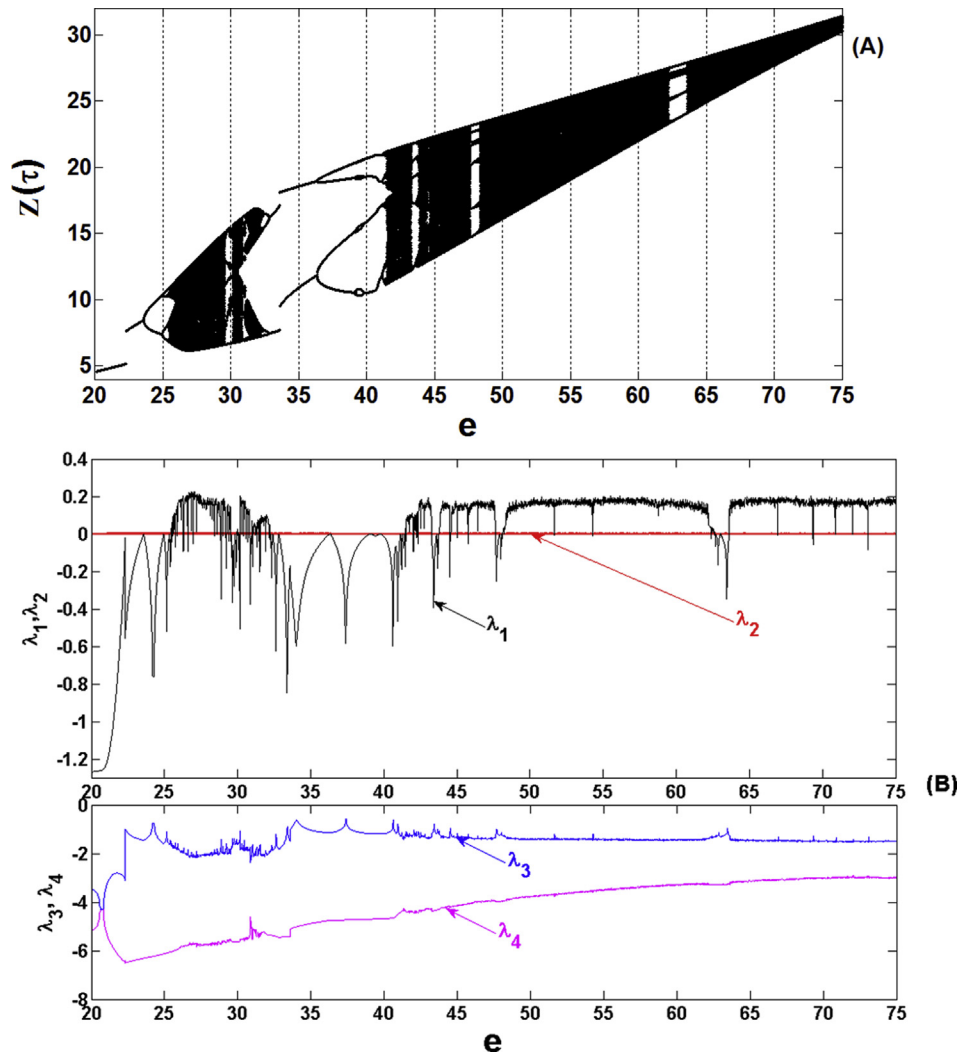


Fig. 5. PSpice's Phase diagram showing the Base-voltage as function of the current through the inductor, the amplitude and frequency of the driven source are respectively  $E = 4.5 \text{ V}$  and  $f = 5 \text{ MHz}$ , while the inductance of the coil is  $L = 75 \text{ }\mu\text{H}$ .

$0.0988$ ,  $\alpha_C = 0.3953$ ,  $\gamma = 4.9411$ ,  $\varepsilon = 4.80$ ,  $\mu = 3.140$ ,  $\alpha_1 = 0.3$ , and  $\alpha_2 = 0.95$ , and control parameter  $e$  (normalized amplitude of the driven source) varying from 20 to 75, we have calculated spectrum of Lyapunov exponents numerically, using the algorithm proposed by Wolf and collaborators [40]. The bifurcation diagram and that corresponding

spectrum of Lyapunov exponents are presented in Fig. 6A, B. The system under investigations is a third order one with a driven source. When calculating the Lyapunov exponents following the algorithm proposed in [40], the phase of the driven source is considered as another dynamic quantity and therefore the four Lyapunov exponents are calculated. It is



**Fig. 6.** Bifurcation diagram (A) showing the local maximum of the coordinate  $z(\tau)$  and the corresponding spectrum of four Lyapunov exponents (B) versus the normalized amplitude  $e$  in the range  $20 \leq e \leq 75$ . The rest of parameter values are taken to be  $\alpha_b = 0.0988$ ,  $\alpha_c = 0.3953$ ,  $\gamma = 4.9411$ ,  $\varepsilon = 4.80$ ,  $\mu = 3.140$ ,  $\alpha_1 = 0.3$ ,  $\alpha_2 = 0.95$ . Notice the positive values of the Lyapunov exponent  $\lambda_1$  where the system is in chaotic motion.

observed on the Fig. 6B that the Lyapunov exponent in the fourth direction (related to the phase of the driven source) is approximately equal to zero. As the amplitude of the external source increases, it can be denoted that the dynamic of the circuit evolves from regular to chaotic behavior, or vice versa through the splitting and reverse splitting of periods. To facilitate the reproduction of our results, complementary Mat-Lab files are made available, also for didactic purpose. This include the programming codes entitled Dynamic\_BJT\_L.m, BJT\_L.m, BIF\_BJT\_L.m, f1.m, f2.m and f3.m). Similarly, for the calculation of the Lyapunov exponent, the Fortran90 code file entitled Lyapunov\_Exponents\_BJT\_L.f90 is provided.

These observations are furthermore sustained by the phase portraits in the  $(x, z)$ -phase space and the corresponding graphs of fast Fourier transform (fft), for some values of  $e$  (Fig. 7). As  $e$  increases, phase portraits and fft-graphs change from quasi-sinusoidal oscillations to chaos via period doubling sequences (period-1 — period-2 — period-4 — chaos), identical to similar sequences seeable on the bifurcations diagrams in Fig. 6A, for the same parameter's values. A perfect match is observed on Fig. 6 between the bifurcation diagram and the Lyapunov exponent, which is positive when the system has infinite periods in the phase space, a signature for chaotic motions.

To obtain more information on the complexity of this simple circuit,

we provide in Fig. 8, the two-dimensional projections  $(y, x)$  and  $(y, z)$ -phase diagrams, a temporal representation, as well as the double-sided Poincaré section projected onto the plane  $x = 0$ . The shapes of the Poincaré map section as well as the wide spectrum of infinite periodicity are also some characteristics of chaotic motions.

### 5.2. Multistability and coexistence of attractors

The detection of hysteretic dynamic windows on bifurcation diagrams is a signature of the existence of multistability, when the parameters or initial conditions of a system vary. Such effect can be noted in our case when the amplitude of the external source varies. Let us consider the bifurcation diagrams in Fig. 6 and do a suitable zoom on the window of  $e$  in the range  $30 \leq e \leq 34$ . The result is depicted by Fig. 9. Here, it can be observed that the long-term behavior of the system depends essentially on the choice of the initial conditions, which leads to the interesting and striking phenomenon of multistability marked by the coexistence of attractors. To justify that the present circuit exhibits multiple coexisting solutions, parallel branches bifurcations and the corresponding largest Lyapunov exponents have been plotted (Fig. 9). This figure denotes the superimposed graphical results where the diagram in magenta (resp. blue) is plotted by increasing the values of  $e$  for the initial

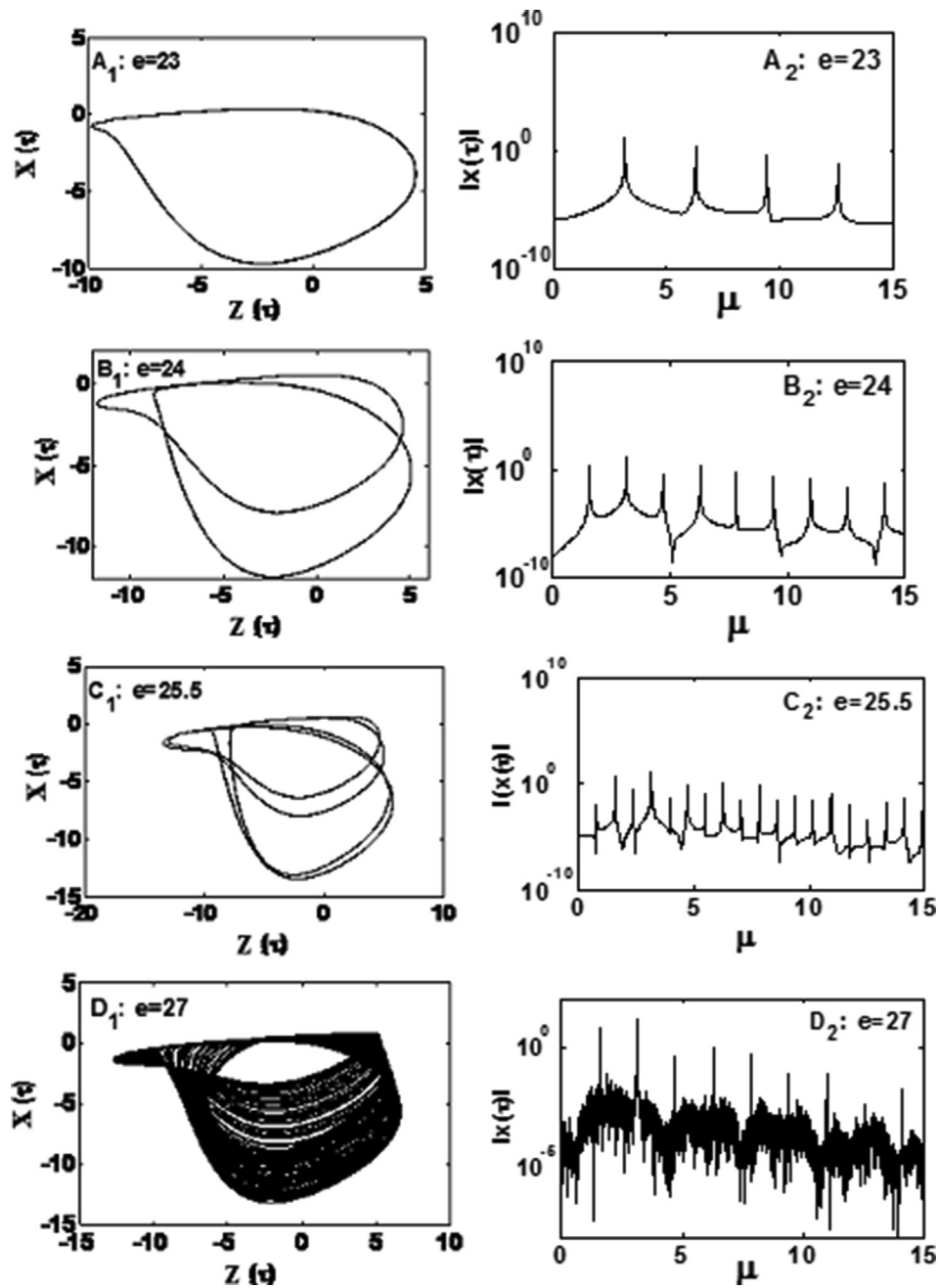


Fig. 7. - phase portraits and the corresponding  $|x|$ - Fast Fourier Transform showing routes to chaos through the inverse splitting of periods in the circuit. This is obtained by varying the normalized amplitude's parameter  $e$ : ( $A_1, A_2$ ) Period-1 for  $e = 23$ , ( $B_1, B_2$ ) Period-2 for  $e = 24$ , ( $C_1, C_2$ ) Period-4 for  $e = 25.5$ , and ( $D_1, D_2$ ) chaotic motion for  $e = 27$ .

states  $X_{01} = (4.0, -10.0, 0.0)$  (resp.  $X_{02} = (2.0, -10.0, 0.0)$ ).

To confirm the previous results, it is shown in Fig. 10 ( $A_1, A_2, B_1, B_2$ ) the coexistence of different asymmetric periodic and chaotic attractors obtained for the same set of parameters values and the corresponding different initial conditions.

According to [41], it is important to identify the presence of such attractors to avoid unexpected and potentially sudden transitions to undesirable dynamics that can be disastrous to some structures or systems in engineering.

### 5.3. Influence of the parasitic capacitances with the frequency of driven source

The present circuit can be used to better show and explain to scholars

differences in small signal equivalent circuits of a BJT at low respectively at high frequencies. Driven by an external source, two different behaviors of the semiconductor junctions in the BJT can be observed. At low frequencies, the voltage-current relation of the whole circuit is limited to one single ODE due to the presence of the coil:

$$L \frac{di_L}{dt} = - (v_{BE} + v_{BC}) - R_C i_L + E \sin(2\pi ft). \quad (16)$$

Thus, the required conditions for chaotic oscillations will not be satisfied. At high frequencies ( $\sim$ MHz), the parasitic capacitances appear due to the Miller effect at the BE and BC junctions of the active element (BJT) according to Giacoletto model. Their presence completes the condition for obtaining two more ODEs, so that the system can be described by Eq. (1) which justifies the appearance of chaotic motions.

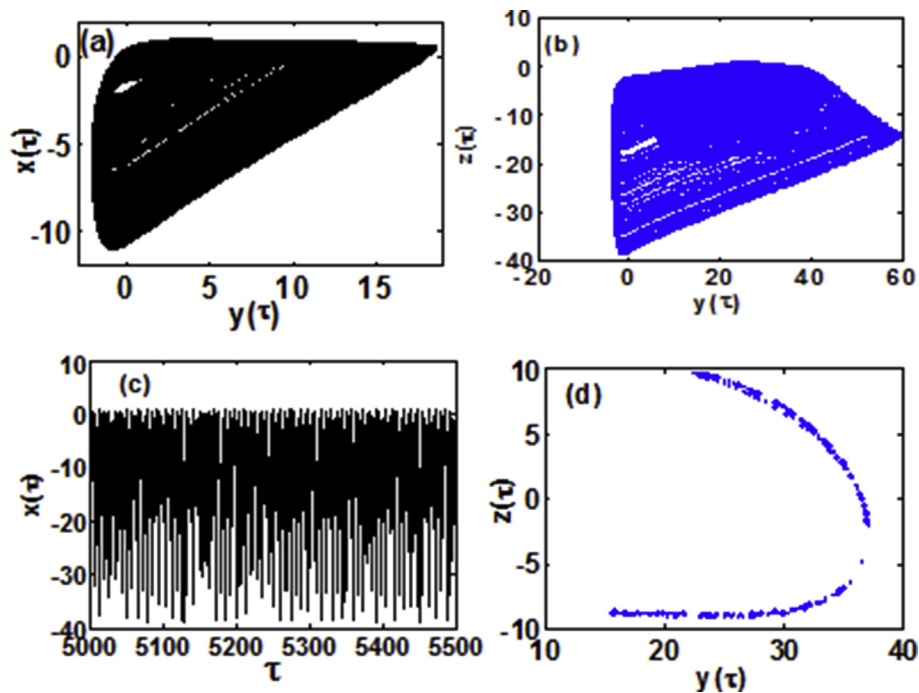


Fig. 8. Two dimensional projections of the asymmetric chaotic attractor (a)–(b) illustrating the complexity of the system in the plan (y, x) and (y, z) respectively; (x)-plan time series (c) and the corresponding double-sided Poincaré section (d) in the plane  $x = 0$  for  $\epsilon = 50$ .

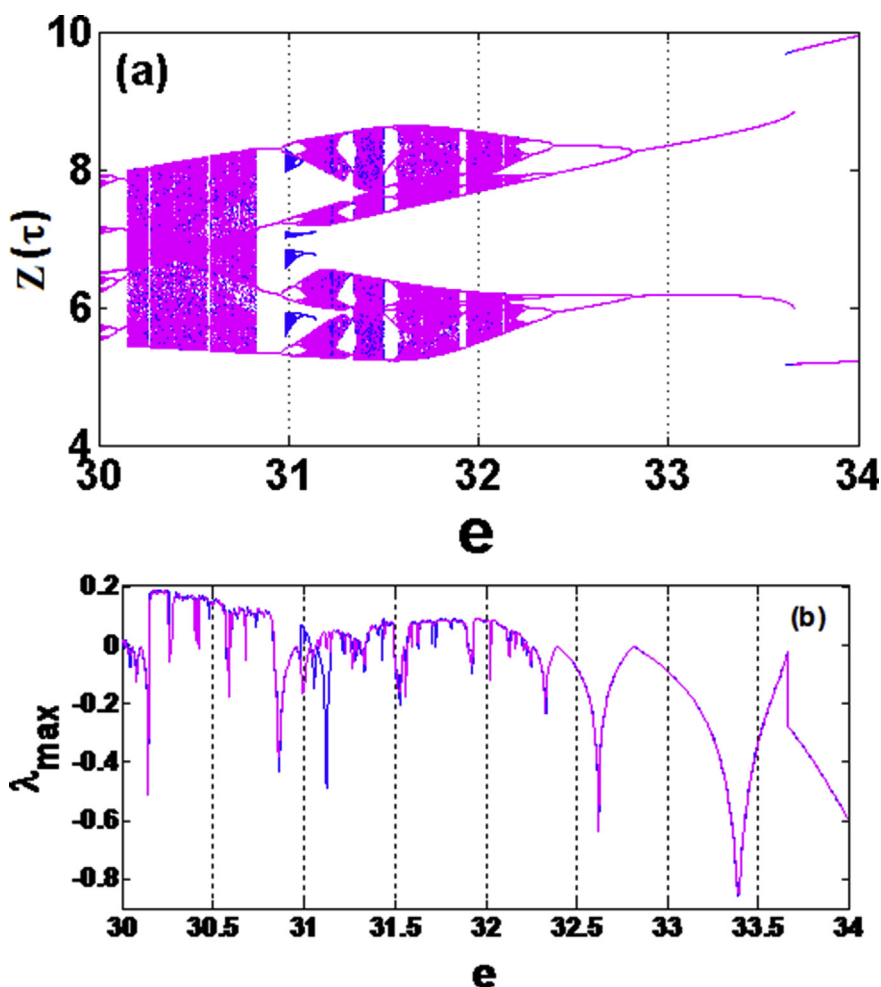
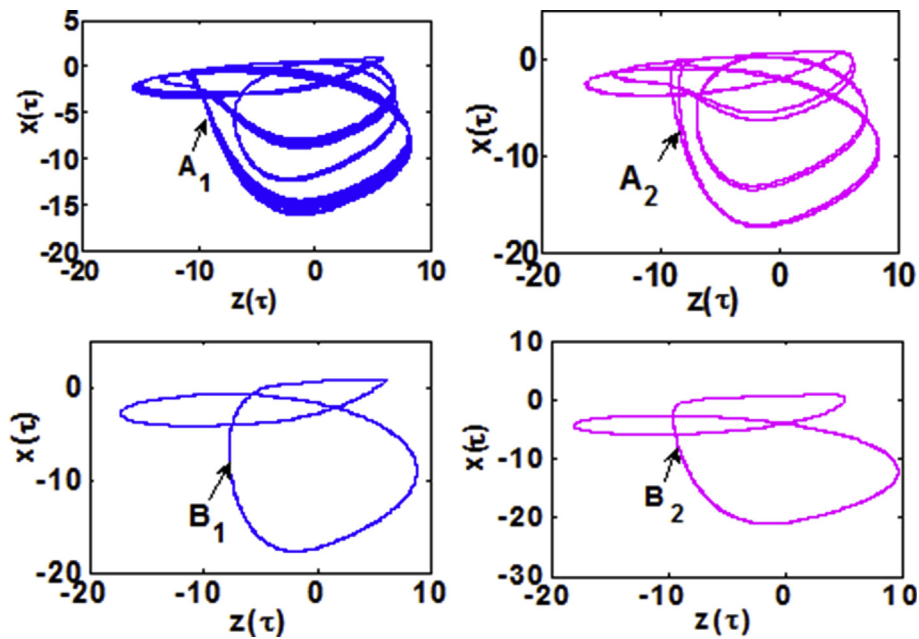


Fig. 9. (a) Coexisting bifurcations' windows and (b) the corresponding largest Lyapunov exponents ( $\lambda_{max}$ ) for the normalized amplitude in the range  $30 \leq e \leq 34$ . Two different coexisting asymmetric solutions can be obtained depending on the value of parameter  $e$  as well as the choice of initial states. Magenta (resp. blue) diagrams correspond to increasing the values of  $e$  starting from the different initial states  $X_{01} = (4.0, -10.0, 0.0)$  (resp.  $X_{02} = (2.0, -10.0, 0.0)$ ). The remaining parameter values are  $\alpha_B = 0.0988$ ,  $\alpha_C = 0.3953$ ,  $\gamma = 4.9411$ ,  $\epsilon = 4.80$ ,  $\mu = 3.140$ ,  $\alpha_1 = 0.3$ ,  $\alpha_2 = 0.95$ .



**Fig. 10.** Coexistence of different asymmetric attractors: Chaotic attractor ( $A_1$ ) and period-8 limit cycles ( $A_2$ ) for  $e = 31$  with initial conditions  $(4.00, -10.0, 0.00)$  and  $(2.00, -10.0, 0.00)$  respectively; ( $B_1, B_2$ ) two different period-1 limit cycles for  $e = 33.63$  with initial conditions  $(-1.40, -10.0, 0.00), (-5.00, -10.0, 0.00)$  respectively. The rest of parameters are the same used to plot Fig. 6.

Hence, the effects of parasitic capacitances are directly related to the frequency of the external source.

Maintaining the parameter values to  $\alpha_B = 0.0988, \alpha_C = 0.3953, \gamma = 4.9411, \varepsilon = 4.80, \mu = 3.140, \alpha_1 = 0.3, \alpha_2 = 0.95$ , a gradual increase of the frequency (increase of  $\mu$ ) until the order of  $\sim$ MHz drives in resonance and the circuit becomes a potential seat of quasi-periodic oscillations and chaotic motion, through the sequences of the inverse splitting of periods (See Fig. 11).

A qualitative changing behavior (bifurcation) is also observed for a critical value of  $\mu$  between 1.358 and 1.359. The richness of the dynamic

of our circuit can be seen in another phenomenon which appears when we monitor the bifurcation diagrams thanks to the ratio of the BE and the BC parasitic capacitances (parameter “ $\varepsilon$ ”). This leads to the sequence of appearance and disappearance of periodic or chaotic orbits [42]. Period-doubling scenario including period-2 primary bubbles to chaotic bubbles through period-4 bubbles is presented in Fig. 12 for the control parameter in the range  $2 \leq \varepsilon \leq 7$  and a systematic variation of the parameter  $e$ . For  $e = 24$ , a period-2 bubble is observed and the branch develops a stable period-4 bubble at  $e = 25.2$ . As  $e$  is further increased, more bubbles are created at  $e = 25.4$  until an infinitely

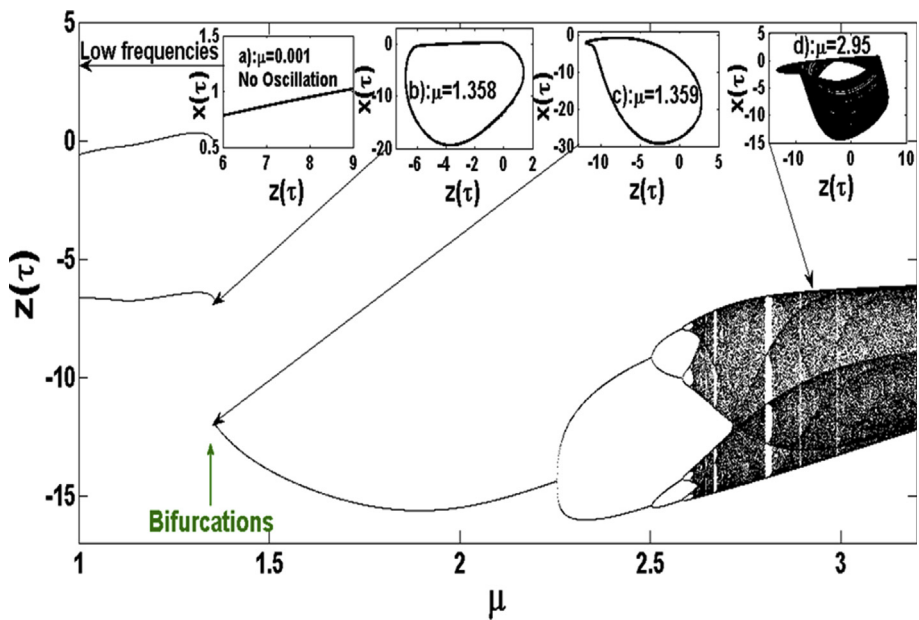


**Fig. 11.** Bifurcation diagram showing the local maximum of the coordinate  $z(\tau)$  versus the normalized frequency  $\mu$  in the range  $1.0 \leq \mu \leq 3.2$ . The rest of parameter values are defined in the text. Notice four different phase portraits with no oscillation for  $\mu = 0.001$  (low frequency):  $\mu = 1.358$  and  $\mu = 1.359$  to show the critical value at which a bifurcation occurs and chaotic motion for  $\mu = 2.95$ .

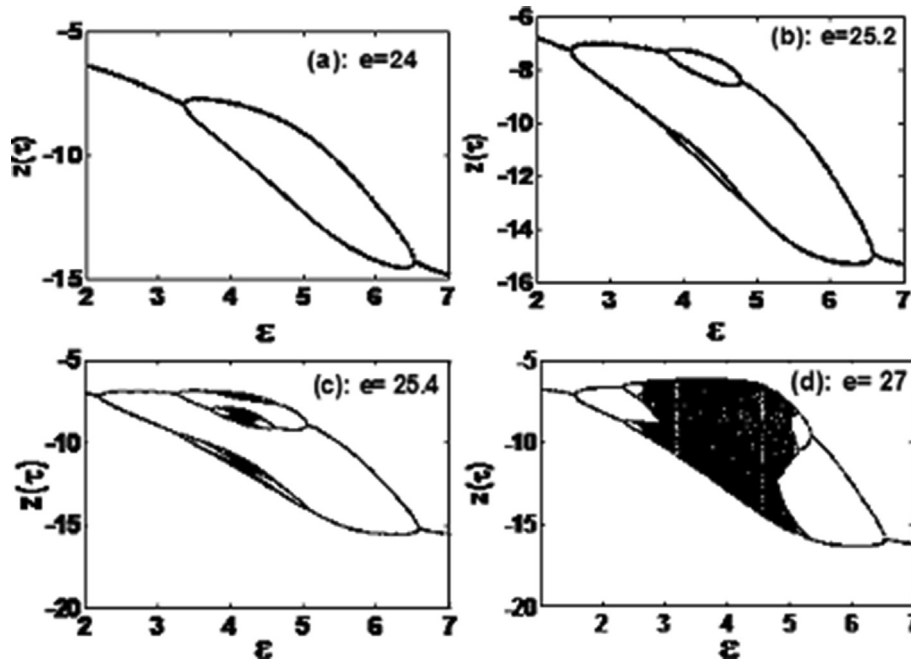


Fig. 12. Bifurcation diagrams showing local maximum of the coordinate  $z(\tau)$  versus the control parameter  $\epsilon$  for remerging Feigenbaum trees (bubbling): (a) primary bubble fore  $\epsilon = 24$ ; (b) period-4 bubble fore  $\epsilon = 25.2$ ; (c) chaotic bubbles for  $\epsilon = 25.4$  and (d) Full Feigenbaum remerging trees at  $\epsilon = 27$ . The parameters values are:  $\alpha_B = 0.0988$ ,  $\alpha_C = 0.3953$ ,  $\gamma = 4.9411$ ,  $\mu = 3.140$ ,  $\alpha_1 = 0.3$ ,  $\alpha_2 = 0.95$  and  $\epsilon$  in the range  $2 \leq \epsilon \leq 7$ .

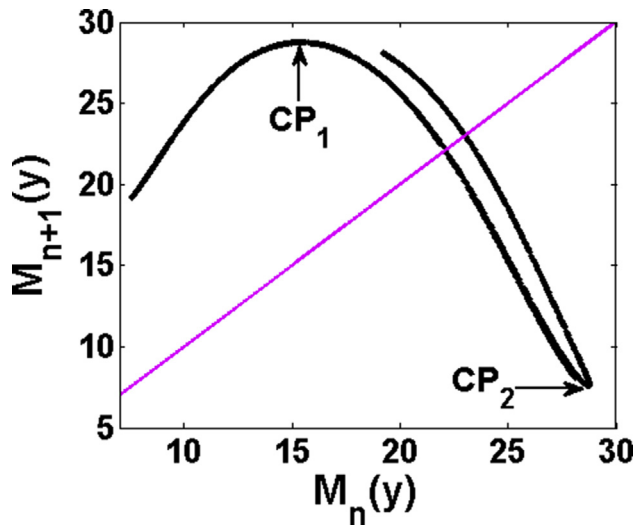


Fig. 13. First-return map of the maxima of the coordinate  $y(\tau)$ . This map is indicative of one-dimensional maps with two critical points confirming the occurrence of antimonotonicity phenomenon in our circuit. The parameters values are the same as in Fig. 12.

Feigenbaum trees finally occurs for  $\epsilon = 27$ .

We provide the first return map of the coordinate  $y$ , this is  $M_{n+1}(y) = f(M_n(y))$  in Fig. 13. This map is typical of one-dimensional

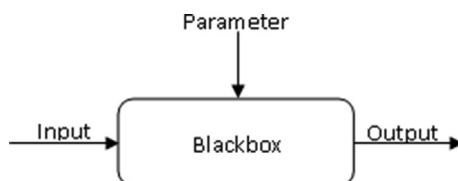


Fig. 14. Abstract black-box model of Fig. 1.

map with two critical points  $P_1$  and  $P_2$  which support the occurrence of antimonotonicity in our system [42, 43].

### 6. Conclusion

In this scientific contribution, we have presented an experimental simple two-components circuit consisting of a coil and a BJT with short-circuited BE electrodes, and adequate for didactic purpose. In case of a black-box consideration of Fig. 1, the whole system could be reported as Fig. 14 with following description of the functioning: when parameter equal HF, then Eq. (1), else Eq. (16).

We could answer without abstraction and in details the ambiguous ‘WHY question’ following the change in the output with that of the parameter. To achieve this, we used Fig. 2, to make the inner of the system available for inspection, and therefore to prove that, although the circuit is basically not an oscillator, it generates very complex signals at resonant frequencies, under the effect of an external sinusoidal driving force. Using an appropriately HF model transistor, the circuit could be modeled mathematically. This model circuit can help scholars to experience the appearance of high frequency dependent virtual capacitances at semiconductors’ junctions. The analysis of the system has shown a great influence of the effect of stray capacitances internal to the BJT, on the operation of the proposed circuit. They can give rise to harmonic and chaotic oscillations or destroy them appropriately according to the frequency of oscillations. Despite the simplicity of the circuit, it exhibits the unusual characteristics of antimonotonicity and coexisting attractors, materialized by parallel bifurcations for a set of circuit parameters and different initial conditions. By using two components that are simple and familiar to scholars to expose various aspects of nonlinear dynamics through the exploitation of classical nonlinear analysis tools such as the bifurcation diagrams, the calculation of Lyapunov exponents, the stability analysis, phase space trajectories, Poincaré map section and frequency spectra, we hope to give a supplementary tool for the introduction of nonlinear dynamics at lower academic level. The present circuit is surely one of the simplest that can suitably work at HF and present a very complex dynamic under the effect of parasitic capacitances.

## Declarations

### Author contribution statement

François C. Talla: Performed the experiments; Analyzed and interpreted the data; Wrote the paper.

Robert Tchitnga: Conceived and designed the experiments; Contributed reagents, materials, analysis tools or data; Wrote the paper.

Romantic Kengne: Performed the experiments; Analyzed and interpreted the data.

Bonaventure Nana: Analyzed and interpreted the data; Wrote the paper.

Anaëlet Fomethé: Contributed reagents, materials, analysis tools or data; Wrote the paper.

### Funding statement

This research did not receive any specific grant from funding agencies in the public, commercial, or not-for-profit sectors.

### Competing interest statement

The authors declare no conflict of interest.

### Additional information

Supplementary content related to this article has been published online at <https://doi.org/10.1016/j.heliyon.2019.e02715>.

## Acknowledgements

F.C.T. thanks Mr. A. Nguomkam Negou from the LAIA, Department of Electrical Engineering, IUT-FV Bandjoun, Cameroon, for constructive discussions during his work. R.T. expresses his gratitude to Hameg Instrument GmbH, Mainhausen, Germany for having provided his research group with the oscilloscope HM 205-3 mentioned in the experimental section of this paper.

## References

- C. Aissi, Introducing chaotic circuits in an undergraduate electronic course. Proceedings of the 2002 ASEE Gulf-Southwest Annual Conference, the University of Louisiana at Lafayette, 2002 Mar 20, pp. 1–8.
- M.A. Perc, Introducing nonlinear time series analysis in undergraduate courses, *FIZIKA A-ZAGREB* 15 (2) (2006) 91–112. [http://fizika.hfd.hr/fizika\\_a/av06/a15p091.pdf](http://fizika.hfd.hr/fizika_a/av06/a15p091.pdf). Accessed on 18/06/2019; 11:41.
- L.O. Chua, The genesis of Chua's circuit, 46, Hirzel-Verlag, Stuttgart, 1992, pp. 250–257 (4), <https://www-inst.cs.berkeley.edu/~ee129/sp10/handouts/GenesisChuasCircuit.pdf>. Accessed on 03/05/2019, 14:03.
- E.N. Lorenz, Deterministic nonperiodic flow, *J. Atmos. Sci.* 20 (2) (1963) 130–141. [https://journals.ametsoc.org/doi/pdf/10.1175/1520-0469\(1963\)020%3C0130%3Adnf%3E2.0.co%3B2](https://journals.ametsoc.org/doi/pdf/10.1175/1520-0469(1963)020%3C0130%3Adnf%3E2.0.co%3B2). Accessed on 18/06/2019; 12:38.
- B.J. West, *Fractal physiology and chaos in medicine*, in: World Scientific, second ed., 16, Nov 2013, p. 344.
- V. Petrov, V. Gaspar, J. Masere, K. Showalter, Controlling chaos in the Belousov–Zhabotinsky reaction, *Nature* 361 (6409) (1993) 240–243.
- B. Nana, S.B. Yamgoué, R. Tchitnga, P. Woafu, On the modeling of the dynamics of electrical hair clippers, *Chaos, Solitons Fractals* 112 (2018) 14–23.
- Y. Nakamura, A. Sekiguchi, The chaotic mobile robot, *IEEE Trans. Robot. Autom.* 17 (6) (2001) 898–904.
- A. Fichera, C. Losenno, A. Pagano, Clustering of chaotic dynamics of a lean gas-turbine combustor, *Appl. Energy* 69 (2) (2001) 101–117.
- I.V. Ermakov, S.T. Kingni, V.Z. Tronciu, J. Danckaert, Chaotic semiconductor ring lasers subject to optical feedback: applications to chaos-based communications, *Opt. Commun.* 286 (2013) 265–272.
- T. Nguazon, T. Nguekeng, R. Tchitnga, A. Fomethé, Simple finite-time sliding mode control approach for Jerk circuits, *Adv. Mech. Eng.* 11 (1) (2019) 1–11.
- R. Kengne, R. Tchitnga, A. Mezatio, A. Fomethé, G. Litak, Finite-time synchronization of fractional-order simplest two-component chaotic oscillators: application to digital cryptography, *Eur. Phys. J. B* 90 (5) (2017) 1–10, 88-Article ID 839038.
- Y. Wang, X. Liao, T. Xiang, K.-W. Wong, D. Yang, Cryptanalysis and improvement on a block cryptosystem based on iteration a chaotic map, *Phys. Lett. A* 363 (4) (2007) 277–281.
- H. Bao, J.H. Park, J. Cao, Synchronization of fractional-order delayed neural networks with hybrid coupling, *Complexity* 21 (S1) (2016) 106–112.
- M. Inoue, A. Nagayoshi, A chaos neuro-computer, *Phys. Lett. A* 158 (8) (1991) 373–376.
- R. Tchitnga, H.B. Fotsin, B. Nana, P.H. Louodop Fotso, P. Woafu, Hartley's oscillator: the simplest chaotic two-component circuit, *Chaos, Solitons Fractals* 45 (3) (2012) 306–313.
- M.P. Kennedy, Chaos in the colpitts oscillator, *IEEE Trans. Circuits Syst.* 41 (11) (1994) 771–774.
- A.S. Elwakil, M.P. Kennedy, A family of Colpitts-like chaotic oscillators, *J. Frankl. Inst.* 336 (4) (1999) 687–700.
- A. Namajunas, A. Tamasevicius, Modified Wien–Bridge oscillator for chaos, *Electron. Lett.* 31 (5) (1995) 335–336.
- R. Tchitnga, R. Zebaze Nanfa'a, F.B. Pelap, P. Louodop, P. Woafu, A novel high-frequency interpretation of a general purpose Op-Amp-based negative resistance for chaotic vibrations in a simple a priori nonchaotic circuit, *J. Vib. Control* 23 (5) (2017) 744–751.
- A.S. Elwakil, A.M. Soliman, Two twin-T based op amp oscillators modified for chaos, *J. Frankl. Inst.* 335 (4) (1998) 771–787.
- J.C. Sprott, A proposed standard for the publication of new chaotic systems, *Int. J. Bifurcat. Chaos* 21 (09) (2011) 2391–2394.
- B. Muthuswamy, L.O. Chua, Simplest chaotic circuit, *Int. J. Bifurcat. Chaos* 20 (5) (2010) 1567–1580.
- V.T. Pham, A. Buscarino, L. Fortuna, M. Frasca, Simple memristive time-delay chaotic systems, *Int. J. Bifurcat. Chaos* 23 (4) (2013), 1350073–81.
- Bo.-C. Bao, F.-W. Hu, Z. Liu, J.-P. Xu, Mapping equivalent approach to analysis and realization of memristor-based dynamical circuit, *Chin. Phys. B* 23 (7) (2014), 070503.
- Bo.-C. Bao, M. Chen, H. Bao, Q. Xu, Extreme multistability in a memristive circuit, *Electron. Lett.* 52 (12) (2016) 1008–1010.
- T. Matsumoto, L. Chua, S. Tanaka, Simplest chaotic nonautonomous circuit, *Phys. Rev. A* 30 (2) (1984) 1155–1157.
- A. Azzouz, M. Hasler, Orbits of the RL-diode circuit, *IEEE Trans. Circuits Syst.* 37 (11) (1990) 1330–1338.
- E. Lindberg, K. Murali, A. Tamasevicius, The smallest transistor-based nonautonomous chaotic circuit, *IEEE Trans. Circ. Syst.—II: Express Briefs* 52 (10) (2005) 661–664.
- A. Elshabini-Riad, F.W. Stephenson, A. Bhutta Imran, Electrical equivalent circuit models and device simulators for semiconductor devices, in: C. Dorf Richard (Ed.), *The Electrical Engineering Handbook*, CRC Press LLC, Boca Raton, 2000.
- O. Tsakiridis, D. Syvridis, E. Zervas, J. Stonham, Chaotic operation of a colpitts oscillator in the presence of parasitic capacitances, *WSEAS Trans. Electron.* 1 (2) (2004) 416–421. <http://wseas.us/e-library/conferences/austria2004/papers/482-308.pdf>. Accessed on 22/05/2019, 20:45.
- A.S. Dimitriev, S. Starkov, Experiments on direct chaotic communications in microwave band, *Int. J. Bifurcat. Chaos* 13 (06) (2003) 1495–1507.
- M.P. Kennedy, On the relationship between the chaotic Colpitts oscillator and Chua's oscillator, *IEEE Trans. Circ. Syst.—I: Fundamental Theory and Applications* 42 (6) (1995) 376–379.
- M. Karakayis, Y. Uyaroglu, Synchronization of Two Chaotic Behaviour Colpitts Oscillator, *5<sup>th</sup> International Advanced Technologies Symposium (IATS'09)*, 13–15, Karabuk, Turkey, 2009.
- J. Zhang, Investigation of Chaos and Nonlinear Dynamical Behaviour in Two Different Self-Driven Oscillators, PhD Thesis, University of London, 2001, p. 197. <https://ethos.bl.uk/OrderDetails.do?uin=uk.bl.ethos.368957>.
- G.M. Maggio, O. De Feo, M.P. Kennedy, Nonlinear analysis of the Colpitts oscillator and applications to design, *IEEE Trans. Circuits Syst.* 46 (9) (1999) 1118–1130.
- M.P. Haniias, I.L. Giannis, G.S. Tombras, Chaotic operation by a single transistor circuit in the reverse active region, *Chaos: An Interdisciplinary Journal of Nonlinear Science* 20 (1) (2010), 013105.
- J. Guckenheimer, P. Holmes, Local bifurcations, in: *Nonlinear Oscillations, Dynamical Systems, and Bifurcations of Vector Fields*. Applied Mathematical Sciences 42, Springer, New York, 1983.
- L.O. Chua, C.W. Wu, A. Huang, G.-Q. Zhong, A universal circuit for studying and generating chaos. I. Routes to chaos, *IEEE Trans. Circ. Syst. I: Fundamental Theory and Applications* 40 (10) (1993) 732–744.
- A. Wolf, J.B. Swift, H.L. Swinney, J.A. Wastano, Determining Lyapunov exponents from time series, *Phys. D Nonlinear Phenom.* 16 (3) (1985) 285–317.
- Z. Wei, I. Moroz, J.C. Sprott, A. Akgul, W. Zhang, Hidden hyperchaos and electronic circuit application in a self-exciting homopolar disc dynamo, *Chaos, An Interdisciplinary Journal of Nonlinear Science* 27 (3) (2017), 033101.
- S.P. Dawson, C. Grebogi, J.A. Yorke, I. Kan, H. Koçak, Antimonotonicity: inevitable reversals of period-doubling cascades, *Phys. Lett. A* 162 (3) (1992) 249–254.
- M. Bier, T.C. Bountis, Remerging Feigenbaum trees in dynamical systems, *Phys. Lett. A* 104 (5) (1984) 239–244.